Local Effects in the X-ray Absorption Spectrum of CaCl2, MgCl2, and NaCl Solutions

H. J. Kulik, A. A. Correa Tedesco, E. Schwegler, D. Prendergast, G. Galli

April 12, 2010

Physical Chemistry B

Disclaimer

This document was prepared as an account of work sponsored by an agency of the United States government. Neither the United States government nor Lawrence Livermore National Security, LLC, nor any of their employees makes any warranty, expressed or implied, or assumes any legal liability or responsibility for the accuracy, completeness, or usefulness of any information, apparatus, product, or process disclosed, or represents that its use would not infringe privately owned rights. Reference herein to any specific commercial product, process, or service by trade name, trademark, manufacturer, or otherwise does not necessarily constitute or imply its endorsement, recommendation, or favoring by the United States government or Lawrence Livermore National Security, LLC. The views and opinions of authors expressed herein do not necessarily state or reflect those of the United States government or Lawrence Livermore National Security, LLC, and shall not be used for advertising or product endorsement purposes.

Local effects in the X-ray absorption spectrum of CaCl$_2$, MgCl$_2$, and NaCl solutions

Heather J. Kulik* and Nicola Marzari

Department of Materials Science and Engineering,
Massachusetts Institute of Technology, Cambridge, MA 02139, USA

Alfredo A. Correa and Eric Schwegler

Lawrence Livermore National Laboratory, Livermore, California, 94550, USA

David Prendergast

Lawrence Berkeley National Laboratory, Berkeley, California, 94720, USA

Giulia Galli

Lawrence Livermore National Laboratory, Livermore, California, 94550,
USA and University of California, Davis, California 95616, USA
(Dated: April 12, 2010)

Both first principles molecular dynamics and theoretical X-ray absorption spectroscopy have been used to investigate the aqueous solvation of cations in 0.5 M MgCl$_2$, CaCl$_2$, and NaCl solutions. We focus here on the species-specific effects that Mg^{2+}, Ca^{2+}, and Na$^+$, have on the X-ray absorption spectrum of the respective solutions. For the divalent cations, we find that the hydrogen bonding characteristics of the more rigid magnesium first shell water molecules differ from those in the more flexible solvation shell surrounding calcium. In particular, the first solvation shell water molecules of calcium are accessible to forming acceptor hydrogen bonds, and this results in an enhancement of a post-edge peak near 540 eV. The absence of acceptor hydrogen bonds for magnesium first shell water molecules provides an explanation for the experimental and theoretical observation of a lack of enhancement at the post-main-edge peak. For the sodium monovalent cation we find that the broad tilt angle distribution results in a broadening of post-edge features, despite populations in donor-and-acceptor configurations consistent with calcium. We also present the re-averaged spectra of the MgCl$_2$, CaCl$_2$, and NaCl solutions and show that trends apparent with increasing concentration (0.5 M, 2.0 M, 4.0 M) are consistent with experiment. Finally, we examine more closely both the effect that cation coordination number has on the hydrogen bonding network and the relative perturbation strength of the cations on lone pair oxygen orbitals.

I. INTRODUCTION

Metal cations, such as calcium, magnesium, and sodium, play a vital role in many biological systems, including in signal transduction, chemical bond activation, and the immune system, and the chloride anion is also relevant for maintaining proper osmotic pressure in the cell[1]. Because of the relevance of metal ions in biology, a number of experimental techniques, including X-ray diffraction (XRD)[2–4], extended X-ray absorption fine structure (EXAFS) spectroscopy[5], and neutron diffraction[6, 7] have been used to elucidate the coordination of Ca^{2+}, Mg^{2+}, Na$^+$, and other cations in water. Both XRD[3] and EXAFS results[8] suggest a coordination number between six and eight for Ca^{2+}, while Mg^{2+} has been shown by XRD to be coordinated octahedrally with six water molecules[2], and XRD experiments indicate Na$^+$ is coordinated by four to six water molecules[4].

Importantly, first-principles molecular dynamics calculations were shown to be necessary in order to re-

cover experimentally observed coordination numbers for Mg^{2+}[9], Ca^{2+}[10], and Na$^+$[11]. The force fields employed in classical molecular dynamics calculations tend to overestimate structure and coordination number for the solvation shell of these ions[3, 12]. The exchange rate of water molecules in the first solvation shell of Mg^{2+} was measured experimentally to be 5.3x10^5 s^{-1} [13]. First-principles calculations of exchange rates predict no exchange of Mg^{2+} first solvation shell water molecules on the time scale of the simulations[9], while Ca^{2+} exchange rates are predicted to be on the order of 3x10^{11} s^{-1}[10]. Recently, first principles molecular dynamics studies of the solvation of divalent calcium[10] and magnesium[9] in water have also demonstrated that these divalent cations significantly affect the local geometry and hydrogen bonding network of their solvating water molecules. Namely, they showed that water molecules in both the first solvation shell of magnesium[9] and calcium[10] have a narrowed tilt angle distribution due to the tendency of the water molecules to asymmetrically coordinate the ion through one of the oxygen lone pair orbitals. Conversely, first principles molecular dynamics has determined that monovalent sodium has a much broader tilt angle distribution[11].

Beyond coordination number and exchange events, it is useful to identify the ways in which the electronic

---

*Current address: Lawrence Livermore National Laboratory, Livermore, California, 94550, USA

structure of the first solvation shell water molecules are perturbed by the cation. In addition to the computational first principles molecular dynamics approaches, the experimental technique of core level X-ray absorption spectroscopy (XAS) has been shown to be capable of identifying cation-specific effects in salt solutions[14]. In particular, experimental results have shown that features of the X-ray absorption spectra of monovalent salt solutions are independent of the cation's identity, while there is some species dependence for the divalent cations in salt solutions[14]. The X-ray absorption spectra of these salt solutions show specific enhancements in the pre-edge, main-edge, and post-main-edge peaks with respect to bulk water which, by necessity, must somehow describe the effect that these ions have on the local environment of the water molecules. Theoretical determination of molecular dynamics trajectories and X-ray absorption spectra for these systems can provide a useful link between the features of the spectrum and local properties that include dipoles, ion-water tilt angles, and hydrogen bonding configuration.

In the following, we calculate theoretical X-ray absorption spectra based upon snapshots taken from equilibrated, first principles molecular dynamics on salt solutions containing the cations Ca^{2+}, Mg^{2+}, and Na^+ as well as the counterion Cl^-. We will provide classification of spectral features based upon both tilt angle and hydrogen bonding network for the three cations that helps to explain differences in the experimental spectra for these three cations. We also estimate trends in the spectra with concentration by reweighting our theoretical results. We will show that electronic structure methods are consistent with current experimental results and also provide insight into the differences between the spectra of differing cations.

II. METHODS

Both first principles Born Oppenheimer molecular dynamics (BOMD) and static calculations for determination of X-ray absorption characteristics were carried out with the PBE generalized gradient approximation [15]. The cubic simulation cell contains either one divalent cation, Ca^{2+} or Mg^{2+}, or one monovalent cation, Na^+ (details for Na^+ in parentheses) and two (one) Cl^- anions as counterions as well as 110(52) water molecules, which yields a 0.5 M concentration in a cell that is 14.91(11.74) Å on each side. The valence electronic wavefunctions were described in a plane wave basis that was truncated at 85 Ry, a cutoff commensurate with our use of norm-conserving, nonlocal pseudopotentials of the Hamann-type [16] to represent core electrons. The semicore states, 3p for Ca or 2p for Na and Mg, are also treated as valence electrons. The dynamics simulations, which were carried out using the QBOX code[17], were performed with a 'rigid water model' for Ca and Mg (water in the NaCl simulation was kept flexible) in which the intramolecular geometry of the

water molecules is kept fixed[18]. The elimination of high-frequency ionic motion provides a number of benefits, the most notable of which is allowing for a longer time step of 0.97 fs, while the flexible NaCl simulations were carried out with a 0.48 fs timestep. The production runs for the $CaCl_2$ and $MgCl_2$ cases were both about 28ps in length, and they were collected in the NVE ensemble following an initial equilibration at 340 K using velocity rescaling for about 3 ps. The production runs for the NaCl simulations were about 17 ps in length, and they were collected in the NVT ensemble at 400 K. Elevated temperatures were used, particularly for the flexible water simulations, in response to recent work in the literature that indicates flexible water may be overstructured at room temperature (300 K)[19, 20]. Both $CaCl_2$ and $MgCl_2$ simulations were based upon an initial 1 ns classical molecular dynamics run for NaCl solution with TIP5P water using the Tinker code[21, 22]. The NaCl simulations, which were carried out later, started from configurations generated in previous Na^+ in water simulations[11]. In order to examine the influence of the cations on the electronic structure of water, a localized molecular orbital analysis was performed by obtaining maximally localized Wannier functions (MLWFs)[23] from 15 snapshots for each cation, 5 of which coincide with those used in X-ray absorption calculations (below).

X-ray absorption spectra were calculated for $MgCl_2$, $CaCl_2$, and NaCl salt solutions with an approach implemented in the QUANTUM-ESPRESSO code[24]. Results were obtained from five equally spaced snapshots along the collected molecular dynamics trajectory for each cation. Both first solvation shell waters and randomly selected bulk waters were sampled from each snapshot. In order to model the spectrum of bulk water, six water molecules were randomly selected from each snapshot of each cation where first solvation shell waters were also sampled. A total sample size of 30 bulk water molecules for each different cation simulation is consistent with the sample size chosen in previous work[25]. Following the recent implementation of Prendergast and Galli[25], the final state of the electronic system is calculated in the presence of the core hole, as modeled by a pseudopotential derived from an oxygen atom with one electron removed from the 1s level, which results from the X-ray excitation. The excited electron resides in the first unoccupied band, and the self-consistent potential is used to generate unoccupied levels which are higher in energy than the first excitation. Each excited oxygen atom corresponding to a water molecule in the first solvation shell in the snapshot was calculated following this recipe, as were the oxygen atoms in six additional randomly distributed bulk water molecules in the snapshot. In order to obtain an averaged X-ray absorption spectrum for the total system, these individual contributions were weighted by their relative concentration in the unit cell. We extrapolate to higher concentrations of salt solution, the number of first shell water molecules was reweighted with respect to bulk water using results from

the initial simulation. The matrix elements between the atomic core level and the excited conduction band are computed using a frozen-core approximation[25–28]. A 2x2x2 (3x3x3) k-point mesh was selected for the 110 (52) water cell based upon adequate convergence being obtained with as few as 27 k-points in previous calculations of the X-ray absorption spectra of 32 to 64 water molecules[25]. The computed spectrum is aligned with an onset energy of 535 eV associated with the lowest computed transition and shifted following the scheme in [29]. The computed spectrum is broadened with a Gaussian lineshape that has a 0.15 eV standard deviation. Extensions which minimize the computational cost of this approach and also incorporate nuclear motions have been developed more recently and applied to the solvation of small organic molecules in water[29, 30].

III. RESULTS AND DISCUSSION

A. Structure of first solvation shells

Previous theoretical[9, 10] and experimental work[14] has suggested that Ca^{2+} and Mg^{2+} influence the local structure of water in different ways. In agreement with earlier first-principles molecular dynamics results[9], we observe that Mg^{2+} exhibits a rigid first solvation shell with six water molecules in an octahedral arrangement (see Table I). In contrast, Ca^{2+} has a somewhat flexible first solvation shell with coordination numbers varying between 6 and 8, which is also in agreement with existing results[10]. The dominant configuration for calcium, or 75.5% in our molecular dynamics simulation, is a seven-fold distorted octahedral arrangement. In contrast to the divalent cations, Na^+ is coordinated by fewer water molecules (between 4 and 6) but exhibits the floppiest first solvation shell.
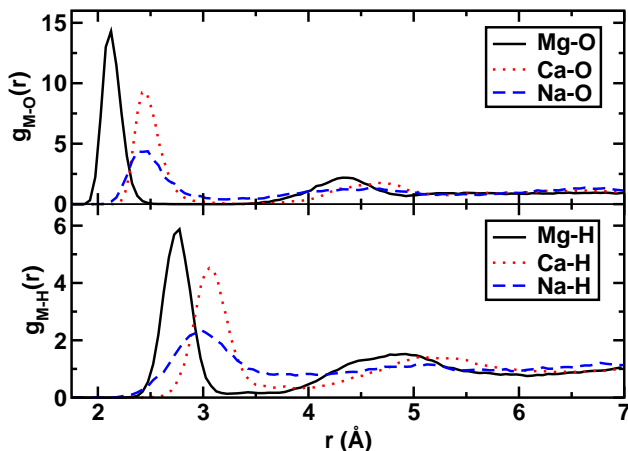

FIG. 1. The cation-oxygen (top) and cation-hydrogen (bottom) radial distribution functions for Mg^{2+} (solid, black), Ca^{2+} (dotted, red), and Na^+ (dashed, blue).

We identify the structural properties of the solvation

shell of these ions in solution from pair radial distribution functions (RDFs), $g_{\alpha\beta}(r)$, which provide a probability of finding an atom of type β at a distance of r from an atom of type α. The radial distribution functions for cation-oxygen and cation-hydrogen atom pairs are shown in Fig. 1. The occupation number in the first solvation shell is determined as the integrated value of $g_{\alpha\beta}(r)$ from 0 to the first minimum in the RDF. The cation-oxygen pairs give an average number in the solvation shell of 6 for Mg^{2+}, 7.1 for Ca^{2+}, and 5.2 for Na^+, with a chosen distance for the first minimum of 2.5 Å, 3.1 Å, and 3.1 Å, respectively. The magnesium-oxygen and magnesium-hydrogen RDFs show the strongest order with the most narrow, well-defined first peak and a strong second peak. Sodium-oxygen and sodium-hydrogen RDFs, and to a lesser extent the calcium cases, exhibit a broader first peak that is shifted outward from the Mg-O value by 0.3 Å, a non-zero density between first and second solvation shells, and a poorly defined second peak (see Fig. 1). The broadening apparent in the first peak of the sodium-hydrogen RDF indicates a decrease in order in the orientations of water molecules as compared to the divalent cation cases; that is, both sodium and calcium exhibit similar M-O peak widths, while the sodium-hydrogen first peak is considerably broadened with respect to that for calcium.

TABLE I. Percentage of single donor (1D), double donor (2D), and double donor plus acceptor (2D+1A) configurations of first shell water molecules separated into the observed coordination environments for Mg^{2+} and Ca^{2+}. These numbers have been renormalized to exclude small miscellaneous contributions from other hydrogen bonding configurations.

CN	Config. %	1D	2D	2D+1A
		Mg		
6	100.0%	18.2%	76.0%	5.8%
		Ca		
6	9.2%	37.9%	57.5%	4.6%
7	75.5%	33.0%	50.9%	16.0%
8	15.3%	30.2%	48.8%	20.9%
Avg.		33.1%	51.2%	15.7%

B. Influence of cations on hydrogen bond network

Commensurate with differing coordination numbers and cationic idenities, we find also underlying differences in the hydrogen bond network for water molecules participating in different solvation shell environments (see Table I). The first solvation shell water molecules of Mg^{2+} are primarily (76%) in a double donor (2D) configuration, with the remainder of hydrogen bond configurations being split between single donor (18%; 1D) and double donor with acceptor (6%; 2D+1A). The relatively strong and rigid binding of the water molecules to the Mg^{2+} center orients the water molecules in such

a way that both hydrogens point outward, available for hydrogen bond donation, but relatively few oxygens are ever accessible to the second shell water molecules as a hydrogen bond acceptor. Furthermore, the relatively ordered movement, or wagging, of the water molecules in the first solvation shell, which was previously observed[9], explains the prevalence of double donor configurations.

Several hydrogen bond network distributions may be determined for Ca^{2+}, each corresponding to differing coordination numbers. The six coordinate Ca^{2+} distribution mirrors Mg^{2+} fairly closely with a dominant (58%) double donor configuration. The double donor percentage for Ca^{2+} is not as high as for Mg^{2+}, and instead a large number of single donor configurations are obtained (38%). However, the share of double donor plus acceptor configurations (5%) is quite comparable to Mg^{2+}. Given the low sample size of six-coordinate Ca^{2+} in the trajectory and the inclusion of snapshots in which the six- to seven-coordinate transition might be taking place, the two cations in the CN=6 configuration are quite similar. As the coordination number for Ca^{2+} increases to seven and eight, a decrease in the number of both single donor and double donor configurations occurs. The double donor plus acceptor configuration weight, however, increases monotonically with increase in coordination number from 5% for CN=6 to 16% for CN=7 and 21% for CN=8. The increased prevalence of 2D+1A configurations is likely due to the longer average Ca^{2+}-OH_2 distances observed for the higher coordination number configurations which make the oxygen available as an acceptor for hydrogen bonds from the second solvation shell (see Fig. 6). That is, moving from the highly symmetrical, octahedral arrangement of six-coordinate Ca^{2+} to a higher coordination number necessarily induces a longer cation-water bond length in the additional water(s). Simple averaging then would suggest that 14%, or one out of seven, of the CN=7 water molecules would be in a 2D+1A configuration, while 25%, or two out of eight, of the CN=8 water molecules would be in the same 2D+1A configuration. The actual observed values are consistent with this rough approximation and also apparently justify the relatively low number of 2D+1A configurations in six-coordinate divalent cations.

The hydrogen bond configuration distribution of first shell water molecules around Na^+ is distinct from those for the divalent cations. The variable coordination number of Na^+ between four and six gives rise to a high number of double donor plus acceptor configurations. Despite a 33% abundance of 2D+1A configurations, there is also a strong contribution from single donor, single acceptor (1D+1A) configurations (32%). The dominant configurations for the divalent cations, single donor or double donor, contribute much less here at about 15% each. The reduced presence of donor hydrogen bonds and higher numbers of acceptor hydrogen bonds (see Fig. 6) results in an enhanced pre-edge peak for sodium, essentially corresponding to the water molecules here

being similar to a water molecule in the gas phase[14].

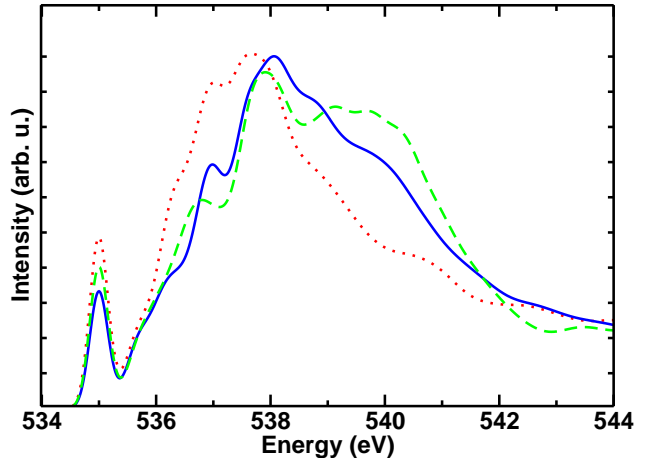## C. Correlation of hydrogen bonds and XAS in divalent cations

FIG. 2. Averaged spectra for water molecules in the first shell of divalent cations (Ca^{2+} or Mg^{2+}) based upon the number of hydrogen bonds: single donor (red, dashed), double donor (blue, solid), and double donor plus acceptor (green, dashed).

Following previous work, one can expect a correlation between the hydrogen bonding network for each water molecule in the first solvation shell of cations and the resulting X-ray absorption spectrum[14]. Our own theoretical measurements of the X-ray absorption spectrum of water molecules in various hydrogen bonding configurations (Fig. 2) confirm this hypothesis. Single donor configurations, which are most like that of an isolated gas phase water molecule, exhibit an enhanced pre-edge feature at around 535 eV with respect to other configuration types. Similarly, the main edge features around 537-538 eV are overall shifted to lower energies and exhibit a narrower energy bandwidth. In contrast, the double donor configurations exhibit a significantly smaller pre-edge feature, a slightly higher energy onset for the edge and a slower decrease in intensity for the post-edge. Most interestingly for the Ca^{2+} simulations, the double donor plus acceptor configurations exhibit some of the features of the single donor case - an enhancement of the pre-edge feature and a first peak which has a maximum at energies close to that for the single donor - but also exhibit a secondary feature in post edge energies around 540-541 eV. This second peak for the double donor plus acceptor configuration is nearly of the same height as the first main edge peak. The differences in the double donor plus acceptor configuration at low energies are likely due to a lower strength of the donor hydrogen bonds, while the high energy feature is likely a feature associated with the acceptor hydrogen bonding. Since the calcium cation simulations have signifi-

cant populations of double donor plus acceptor configurations, the overall CaCl$_2$ XAS results could potentially exhibit features similar to that of the 2D+1A configurations. On the other hand, MgCl$_2$ solutions exhibit a dominantly double donor configuration in the first solvation shell, and the double donor-like features of a strong main edge peak and decreased pre-edge peak are likely to dominate. NaCl solutions, also considered here, are less dominated by a single hydrogen bonding configuration, but these simulations are expected to produce an enhanced pre-edge peak.
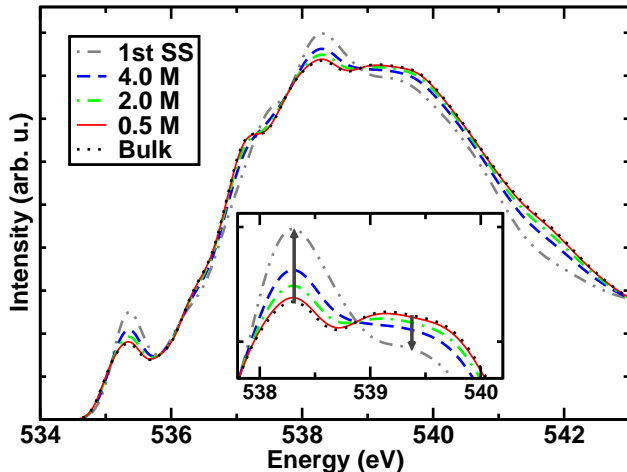
FIG. 3. The X-ray absorption spectra of several concentrations (0.5 M, 2.0 M, 4.0 M) MgCl$_2$ solution referenced against referenced against both bulk water and a spectrum comprised only of water molecules in the first solvation shell of Mg^{2+} (denoted '1st SS'). The 0.5 M concentration reflects that of the simulation, while the higher concentrations were obtained by reweighting the percentage of first shell and bulk water molecules in the spectrum.

In order to compare with experimental X-ray absorption spectra on the MgCl$_2$, CaCl$_2$, and NaCl solutions, we computed the spectrum about an oxygen in one of three categories: first-solvation shell water around the cation, first-solvation shell water around an anion, and randomly selected bulk water not in the first solvation shell of cations or anions. For the first solvation shell of the cation or the anion, we computed the spectrum for all water molecules, while for the bulk case six water molecules were selected at random in each snapshot. We then repeated the calculation for a total of five snapshots for each simulation. The role of the anion is not discussed in depth here because of the high disorder and rapid exchange we observe around the anion, which, while not discussed in depth in this work, is likely to result in chloride solvation shell water molecules exhibiting bulk water-like spectral features[31, 32]. Nevertheless, in general, the chloride ion has enhanced pre-edge and main-edge features with a slight decline at post-edge, with respect to bulk water. We also provide later in the text a comparison of the effect that cations and anions have on the Maximally-localized Wannier func-

tion centers around oxygen atoms in water molecules contained within the first solvation shell. In our simulated X-ray absorption spectra, we consider 0.5 M, the concentration of the molecular dynamics unit cell, 2.0 M, and 4.0 M solutions. For the 0.5 M concentration, we reweighted our spectra from the three categories, bulk, cation water molecules, and anion water molecules, with their approximate population in the cell, or 94, 6, and 10 in the case of MgCl$_2$. In order to approximate higher concentrations, the 2.0 M and 4.0 M spectra were generated by multiplying the cation and anion contributions by four and eight respectively, while reweighting the bulk water molecule contribution. This procedure was also repeated for the other cations. The highest concentration, 4.0 M, corresponds to overlapping of the cation and anion solvation shells, and the calculated spectrum therefore neglects effects on the local structure which might be induced at higher concentrations. The lowest concentration, 0.5 M MgCl$_2$, is virtually indistinguishable from the bulk spectrum (see Fig. 3) even when one zooms in on the main edge features where the greatest variation is likely to occur (see inset of Fig. 3). However, this result is unsurprising since the weight of the solvation shell water molecules at this concentration is only 5% and few features are observed at this concentration experimentally[33]. The apparent overall trend with respect to increasing concentrations at 2.0 M and 4.0 M MgCl$_2$ is an enhancement of the main edge 538 eV peak and a slight decrease in intensity at the post-edge. Such results are in qualitative agreement with the experimental results of Cappa et al.[14], but since we neglect effects of forming contact ion pairs, we do not capture an apparent greater than linear order enhancement in the main edge feature observed in their experiments.

Following confirmation of our ability to theoretically identify the major features of the MgCl$_2$ solution, we wish to determine whether or not we also observe the enhancement of post-edge features in CaCl$_2$ solution. The approximate X-ray absorption spectra for 0.5 M, 2.0 M, and 4.0 M CaCl$_2$ solutions were calculated in a manner equivalent to that which was previously described for MgCl$_2$. As was observed previously, the 0.5 M concentration indicated only slight enhancement at main edge and post-edge features (see Fig. 4). For increasing concentrations, we observe enhancement of main-edge 537-538 eV features much like in MgCl$_2$, however we also observe an enhancement which is about one half as large in magnitude nearer to post edge features at 539-540 eV. This new feature is likely derived nearly exclusively from 2D+1A configurations which are present in much greater concentration in the loosely solvated Ca^{2+} than in the more rigidly solvated Mg^{2+}. These results suggest that relative strengths of main-edge and post-edge enhancement in salt solutions could be used to predict the relative weight of differing hydrogen bonding configuration types.
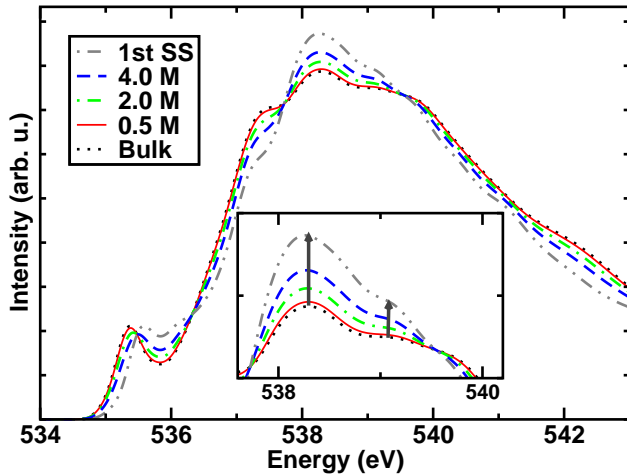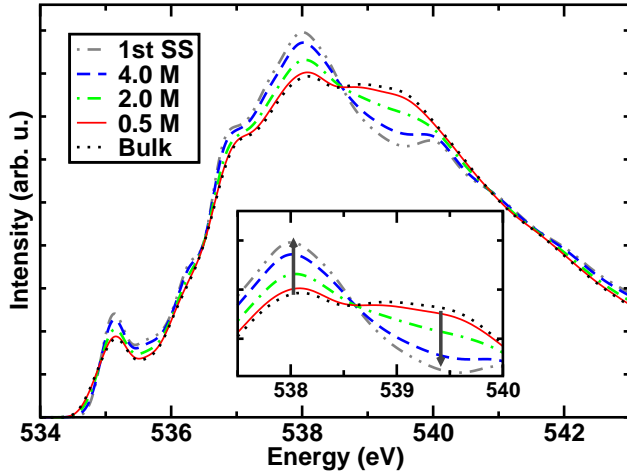
FIG. 4. The X-ray absorption spectra of several concentrations (0.5 M, 2.0 M, 4.0 M) $CaCl_2$ solution referenced against both bulk water and a spectrum comprised only of water molecules in the first solvation shell of Ca^{2+} (denoted '1st SS'). The 0.5 M concentration reflects that of the simulation, while the higher concentrations were obtained by reweighting the percentage of first shell and bulk water molecules in the spectrum.

D. Comparisons of XAS and structure for monovalent and divalent cations

FIG. 5. The X-ray absorption spectra of several concentrations (0.5 M, 2.0 M, 4.0 M) NaCl solution referenced against both bulk water and a spectrum comprised only of water molecules in the first solvation shell of Na^+ (denoted '1st SS'). The 0.5 M concentration reflects that of the simulation, while the higher concentrations were obtained by reweighting the percentage of first shell and bulk water molecules in the spectrum.

It is at first surprising that the experimental spectrum of monovalent sodium and divalent magnesium solutions are so similar since the structure of their solvation shells is very dissimilar[14]. Even more surpris-

ing is that these two spectra exhibit strong similarities while clear discernible differences are present in the relatively similar divalent cases, calcium and magnesium. The solvated magnesium ion exhibits a very rigid solvation shell with a first peak in its radial distribution function (RDF) around 2.1Å (see Fig. 1), a coordination number of six, and no exchange events between water molecules occurring on the timescale accessible by first-principles simulation[13]. Solvated sodium ion, on the other hand, has a first RDF peak at 2.4Å, an average coordination number of 5.2, and frequent exchange events. Our own theoretical spectra of varying concentrations (0.5 M, 2.0 M, and 4.0 M) of NaCl appear to exhibit similar features to that for $MgCl_2$ solutions. In particular, there is an enhancement of the pre-edge and main-edge peaks followed by a significant decline in intensity for post-main-edge features. Nevertheless, the strong similarity of both theoretical and experimental XAS for these fairly dissimilar cations indicates that disparate electronic and structural features can yield features in similar energy windows.

While differences for the divalent cations appear to be driven by differences in the hydrogen bonding network for first-solvation shell water molecules, we considered also the case of monovalent cations, namely sodium. Sodium, like calcium, has a relatively floppy first solvation shell, and therefore might be expected to have a significant population of 2D+1A water molecules. However, solutions of sodium chloride have experimentally[14, 34] been shown to not exhibit enhancement of the post-main-edge peak which we previously attributed to this 2D+1A hydrogen bonding configuration. We previously showed that the distribution of hydrogen bonding types around sodium is significantly different than the distribution around calcium or magnesium. Now, we will consider in further detail the structural properties that distinguish monovalent and divalent cations.

It is important to identify and decouple the roles which hydrogen bond network and coordination might play in differences between Ca^{2+}, Mg^{2+}, and Na^+ spectra. We achieve this by determining radial distribution functions (RDFs) and the average number of hydrogen bonds for Ca^{2+} in a six-coordinate geometry and compare the results to those obtained for Mg^{2+} (see Fig. 6). We observe a relative absence of acceptor bonds corresponding to the nonzero regions of the first RDF peak for both six-coordinated species, while the contribution from acceptor bonds in the nonzero region of the broader first peak of the total Ca^{2+} simulation is apparent. That is, while the relative position of water molecules solvating Ca^{2+} is pushed out with respect to Mg^{2+}, the six-coordinated cations look virtually identical otherwise. Therefore, one would expect that enhancement of the post-edge peak might occur in the X-ray absorption spectra of divalent cations which exhibit coordination numbers and exchange rates similar to Ca^{2+}. Next, comparing to the monovalent Na^+, we see that the acceptor bond concentration is nearly as
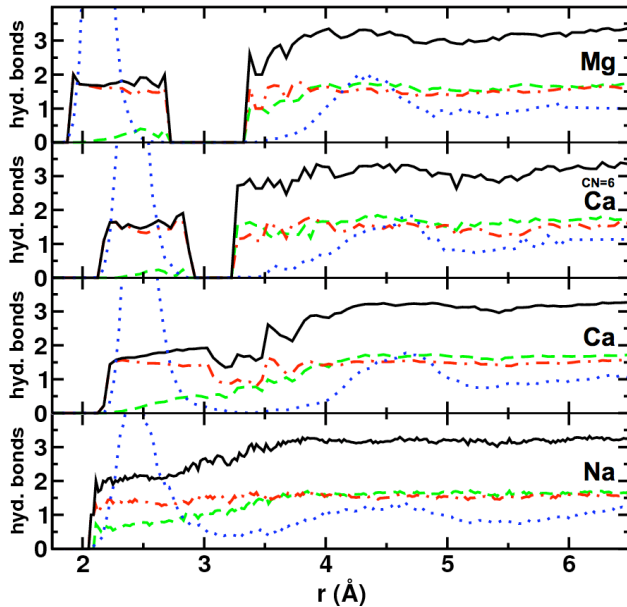
FIG. 6. Comparison of hydrogen bonding (total: solid, black; donor: dot-dashed, red; acceptor: dashed, green)as a function of distance from the cation overlayed with the relevant radial distribution function (dotted, blue). The top graph depicts Mg, which is always six-coordinate, the second graph depicts Ca in a coordination environment of six water molecules, the third graph shows the overall results from a simulation of Ca with an average coordination number of 7.1, and the bottom graph shows the results from a simulation of Na.
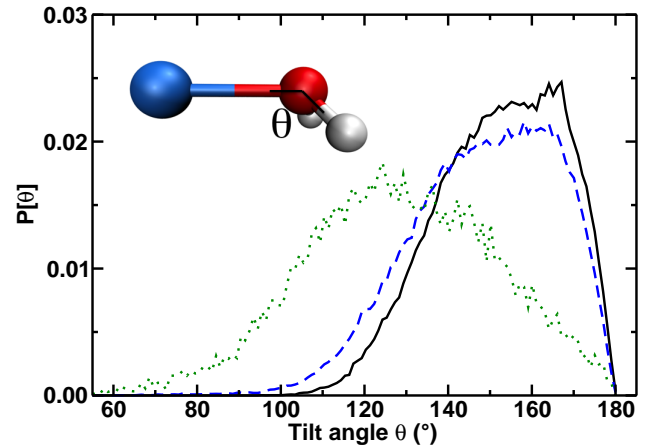

FIG. 7. Comparison of distributions of tilt angles for the divalent cations magnesium (solid black) and calcium (dashed blue) as well as monovalent sodium (green dotted), where the tilt angle is defined as the angle formed between the ion, oxygen, and the bisection of the hydrogens in water. Calcium and magnesium both have well-defined tilt angle distributions, while the sodium tilt angle distribution is broad.
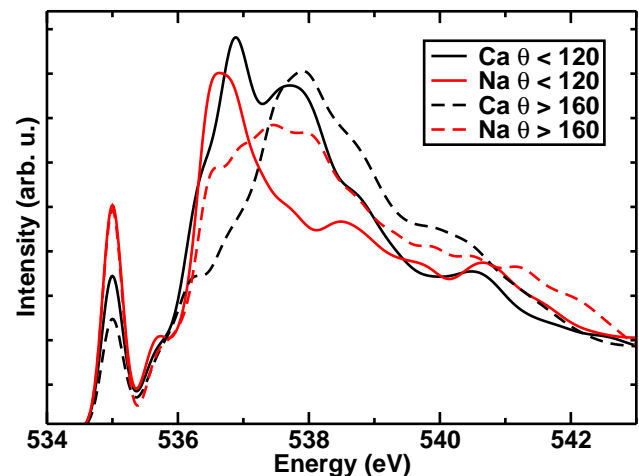

FIG. 8. Comparison of the components of the absorption spectra from small tilt angles (solid line) with large tilt angles (dashed line) for the divalent cation calcium (black) and monovalent cation sodium (red).

high as the donor bond concentration even in the first solvation shell. For shorter ion-oxygen distances comparable in the averaged Ca^{2+} and Na^+ simulations, the acceptor bond concentration is much higher in the sodium case. The higher number of acceptor bonds in sodium indicates less ordered orientation of the water molecules in the sodium first hydration shell because the outward orientation of hydrogens in magnesium and calcium simulations results in very low acceptor bond concentrations. Therefore, the presence of both donor and acceptor bonds in the first solvation shell water molecules is not alone enough to result in post-main-edge peak enhancement.

Sodium does differ from calcium and magnesium in that it has a very broad tilt angle distribution peaked at around 120°, while the two divalent cations have significantly narrower distributions peaked around 160°. The resulting (see Fig. 7). We considered absorption spectra of individual water molecules derived from two extrema for these simulations: large tilt angles close to or greater than 160° and smaller tilt angles around 120° or less. The effect of tilt angle on x-ray absorption spectral features has been previously considered in model systems of water-water interactions[35] and in ion-water 'dimers'[14]. In both cases, some shift of the spectral features towards higher energies occurred for larger tilt angle values. In our work, the water molecules with

larger tilt angle orientations to calcium contribute predominantly to the post-main-edge peak, while the geometries with smaller angles show more pre-edge and main edge contributions. For sodium, on the other hand, we see at large tilt angles a very broad contribution across main-edge and post-main-edge peaks and a significant pre-edge peak, while the smaller angles show a considerably narrower main-edge peak. This result shows that the enhancement of the post-main-edge peak in calcium chloride solutions comes from a few related sources. First, the divalent cations tend to orient a single lone pair towards the ion[9, 10], resulting in a well-defined distribution of tilt angles, while the monovalent cations exhibit a much broader tilt angle distribution.

Secondly, this narrow tilt angle distribution for divalent cations means that the water molecules around calcium spend a significant amount of time in geometric configurations that lend themselves towards specific types of double donor or double donor plus acceptor hydrogen bonding. Finally, the calcium simulations have considerably larger population density at these large tilt angles that contribute to the post-main-edge peak, while, even if the sodium solvation shell water molecules showed a large and well-defined post-main-edge peak at larger tilt angles, they would not contribute significantly to the overall spectrum when averaged over the broad tilt angle distribution.

We also wish to consider the influence that each cation might have on the electronic structure of the solvating water molecules. Maximally localized Wannier functions (MLWFs) can be used to determine the extent to which the cation perturbs each oxygen's molecular orbitals. The distribution of the MLWFs associated with each oxygen of the first solvation shell water molecules is plotted in Fig. 9. The portion of the distribution corresponding to shorter distances (0.25-0.35 Å) is derived from oxygen's lone pair orbitals. The longer distance (0.45-0.55 Å) peak is derived from the Wannier centers on the O-H bond. We observe a clear double-peaked character to the Mg^{2+} simulation results, in agreement with previous simulations that also showed that bulk water would have a broad featureless distribution[10]. From Mg^{2+} to Ca^{2+}, we observe a narrowing in the separation of the two peaks, originally at 0.30 and 0.34 Å, to 0.30 and 0.32 Å. The sodium simulation exhibits a broad peak centered around 0.32 Å, but it lacks significant separation between the two peaks observed in the Mg^{2+} and Ca^{2+} simulations. The bimodal distribution for the oxygen-MLWF center RDFs corresponds to a perturbation of the oxygen lone pair orbital oriented directly towards the cation with respect to that lone pair orbital not oriented towards the cation. Therefore, the trend of decreasing separation of these two peaks from Mg to Ca to Na represent a weakening of the effect that the cation has on the electronic structure, though not necessarily the geometric structure, of surrounding water molecules.

Cappa *et al.* have recently argued [14] that, since monovalent cations all exhibit nearly identical spectral features, the source of these features must be from the counterions. They further suggested that the perturbation of unoccupied oxygen orbitals by the ions is the greatest source of influence on the spectrum and that the anions should have the greatest effect on these orbitals. However, if the Cl^- contribution to the features of the experimental XAS is the most significant, then this effect should be doubly large in the divalent cations where the anions outnumber the cations two-to-one. Nevertheless, earlier results, also from Cappa *et al.*, compared 4M HCl and NaCl solutions and found the HCl spectrum to be very similar to that for bulk water and dissimilar from that of NaCl[32]. The authors suggested that the effects of H^+ and Cl^- roughly
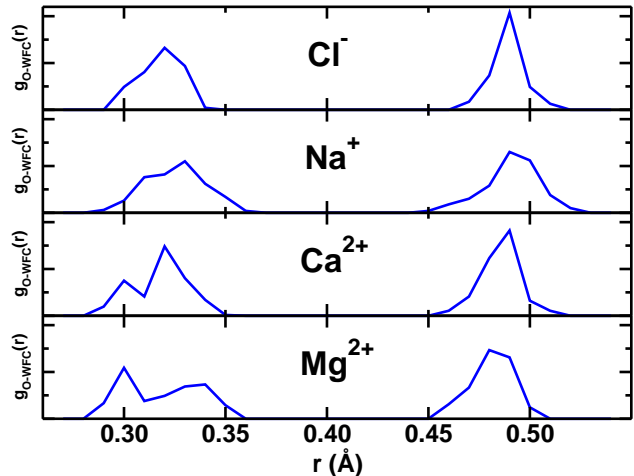

FIG. 9. The oxygen-MLWF center radial distribution functions, g_{O-WFC}, for first shell water molecules in the solvation shells of Mg^{2+}, Ca^{2+}, Na^+, and Cl^-. The Mg^{2+}, Ca^{2+}, and Cl^- results come from rigid water simulations, while the Na^+ results were obtained from snapshots of flexible water simulations.

counteracted each other, yielding spectroscopic features very much like those of bulk water. However, other studies have suggested[31] that the cations contribute more significantly to the features of the X-ray absorption spectrum because they more directly interact with the oxygens of water. Our own results suggest that the influence of Cl^- on the molecular orbitals of first solvation shell oxygen atoms is very small (see Fig. 9). Therefore, we expect the influence of cations to outweigh anions in the X-ray absorption spectrum of salt solutions.

IV. CONCLUSIONS

We have presented the first principles molecular dynamics and theoretical X-ray absorption spectra of $CaCl_2$, $MgCl_2$, and NaCl solutions. Our findings help to explain several previously experimentally observed trends in the spectra of these solutions[14]. First, we found that among the divalent cations, the more rigid magnesium solvation shell prevented water molecules from forming the acceptor hydrogen bonds which were responsible for enhancement of this feature in calcium simulations. Further, we also provided a consistent comparison of oxygen-MLWF center radial distribution functions for the first solvation shell water molecules around Mg^{2+}, Ca^{2+}, and Na^+, which showed that the perturbation of lone pair oxygen orbitals was greatest for Mg^{2+} and smallest for Na^+. We observed that for the monovalent sodium case, the very loose solvation shell here also resulted in a larger number of solvation shell water molecules participating in acceptor hydrogen bonds. However, the broad tilt angle distribution in this monovalent cation with respect to the strongly

peaked tilt angle distribution in the divalent cations explains why the enhanced presence of acceptor hydrogen bonds does not produce a strong feature at the post-main-edge peak. In fact, comparison of the spectra of small tilt angle water molecules with larger tilt angle water molecules showed that the low tilt angle molecules contribute more to the pre-edge and main-edge peaks, while the large angle molecules contribute uniquely to the post-main-edge peak. We not only observed a broad post-main-edge peak in sodium at large angles, but we also noted that the distribution in sodium was heavily weighted towards these lower angles, or the opposite of the case for calcium. The X-ray absorption spectra of sodium and magnesium solutions, therefore, appear very similar, but first principles results show that these spectroscopic features arise for very different reasons.

ACKNOWLEDGMENTS

[1] S. J. Lippard and J. M. Berg. *Curr. Opin. Chem. Biol.*, 4:137 – 139, 2000.

[2] R. Caminiti, G. Licheri, G. Piccaluga, and G. Pinna. *Chem. Phys. Lett.*, 47:275, 1977.

[3] M.M. Probst, T. Radnai, K. Heinzinger, P. Bopp, and B.M. Rode. *J. Phys. Chem.*, 89:753–759, 1985.

[4] N. Skipper and G. Neilson. *J. Phys.: Condens. Matter*, 1:4141, 1989.

[5] J. L. Fulton, S. M. Heald, Y. S. Badyal, and J. M. Simonson. *J. Phys. Chem. A*, 107:4688–4696, 2003.

[6] J. E. Enderby. *Chem. Soc. Rev.*, 24:159, 1995.

[7] N. A. Hewish, G. W. Neilson, and J. E. Enderby. *Nature*, 297:138, 1982.

[8] F. Jalilehvand, D. Spangberg, P. Lindqvist-Reis, K. Hermansson, I. Person, and M. Sandström. *J. Am. Chem. Soc.*, 123:431, 2001.

[9] F. C. Lightstone, E. Schwegler, R. Q. Hood, F. Gygi, and G. Galli. *Chem. Phys. Lett.*, 343:549, 2001.

[10] F. C. Lightstone, E. Schwegler, M. Allesch, F. Gygi, and G. Galli. *ChemPhysChem*, 6:1745, 2005.

[11] J. A. White, E. Schwegler, G. Galli, and F. Gygi. *J. Chem. Phys.*, 113:4668, 2000.

[12] A. Tongraar, K. R. Liedl, and B. M. Rode. *J. Phys. Chem. A*, 101(35):6299–6309, 1997.

[13] J. Neely and R. Connick. *J. Am. Chem. Soc.*, 92(3476), 1970.

[14] C. D. Cappa, J. D. Smith, B. M. Messer, R. C. Cohen, and R. J. Saykally. *J. Phys. Chem. B*, 110:5301, 2006.

[15] J. P. Perdew, K. Burke, and M. Ernzerhof. *Phys. Rev. Lett.*, 77(18):3865–3868, 1996.

[16] N. Troullier and J. L. Martins. *Phys. Rev. B*, 43:1993, 1991.

[17] QBOX, a large-scale parallel implementation of first-principles molecular dynamics, http://eslab.ucdavis.edu.

[18] M. Allesch, E. Schwegler, F. Gygi, and G. Galli. *J. Chem. Phys.*, 120:5192, 2004.

[19] JC Grossman, E Schwegler, EW Draeger, F Gygi, and G Galli. *Journal of Chemical Physics*, 120(1):300–311, 2004.

[20] E Schwegler, JC Grossman, F Gygi, and G Galli. *Journal of Chemical Physics*, 121(11):5400–5409, 2004.

[21] M. W. Mahoney and W. L. Jorgensen. *J. Chem. Phys.*, 112:8910, 2000.

[22] TINKER - Software Tools for Molecular Design, Version 3.9.

[23] N. Marzari and D. Vanderbilt. *Phys. Rev. B*, 56:12847, 1997.

[24] P. Giannozzi, S. Baroni, N. Bonini, M. Calandra, R. Car, C. Cavazzoni, D. Ceresoli, G. L. Chiarotti, M. Cococcioni, I. Dabo, A. Dal Corso, S. de Gironcoli, S. Fabris, G. Fratesi, R. Gebauer, U. Gerstmann, C. Gougoussis, A. Kokalj, M. Lazzeri, L. Martin-Samos, N. Marzari, F. Mauri, R. Mazzarello, S. Paolini, A. Pasquarello, L. Paulatto, C. Sbraccia, S. Scandolo, G. Sclauzero, A. P. Seitsonen, A. Smogunov, P. Umari, and R. M. Wentzcovitch. *J. Phys.: Condens. Matter*, 21:395502, 2009.

[25] D. Prendergast and G. Galli. *Phys. Rev. Lett.*, 21:215502, 2006.

[26] B. Hetenyi, F. D. Angelis, P. Giannozzi, and R. Car. *J. Chem. Phys.*, 120:8632, 2004.

[27] M. Taillefumier, D. Cabaret, A.-M. Flank, and F. Mauri. *Phys. Rev. B*, 66:195107, 2002.

[28] P. E. Blöchl. *Phys. Rev. B*, 50:17953, 1994.

[29] Craig P. Schwartz, Janel S. Uejio, Richard J. Saykally, and David Prendergast. *Journal of Chemical Physics*, 130(18), 2009.

[30] Janel S. Uejio, Craig P. Schwartz, Richard J. Saykally, and David Prendergast. *Chemical Physics Letters*, 467(1-3):195–199, 2008.

[31] M. Cavalleri, L.-A. Naslund, D. C. Edwards, P. Wernet, H. Ogasawara, S. Myneni, L. Ojamae, M. Odelius, A. Nilsson, and L. G. M. Pettersson. *J. Chem. Phys.*, 124(19), 2006.

[32] C. D. Cappa, J. D. Smith, B. M. Messer, R. C. Cohen, and R. J. Saykally. *J. Phys. Chem. B*, 110:1166–1171, 2006.

[33] L.-A. Naslund, D. C. Edwards, P. Wernet, U. Bergmann, H. Ogasawara, L. G. M. Pettersson, S. Myneni, and A. Nilsson. *J. Phys. Chem. A*, 109(27):5995–6002, 2005.

[34] C. D. Cappa, J. D. Smith, K. R. Wilson, B. M. Messer, M. K. Gilles, R. C. Cohen, and R. J. Saykally. *J. Phys. Chem. B*, 109:7046–7052, 2005.

[35] P Wernet, D Nordlund, U Bergmann, M Cavalleri, M Odelius, H Ogasawara, LA Naslund, TK Hirsch, L Ojamae, P Glatzel, LGM Pettersson, and A Nilsson. *Science*, 304(5673):995–999, 2004.